7502 *Biochemistry* **2009,** *48,* 7502–7511
DOI: 10.1021/bi9005336

BIOCHEMISTRY
including biophysical chemistry & molecular biology
Article

Elucidating the Kinetic Mechanism of DNA Polymerization Catalyzed by *Sulfolobus solfataricus* P2 DNA Polymerase B1[†]

Jessica A. Brown[‡,§] and Zucai Suo*[,‡,§,∥,⊥,@]

[‡]*Department of Biochemistry,* [§]*Ohio State Biochemistry Program,* [∥]*Ohio State Biophysics Program,* [⊥]*Molecular, Cellular and Developmental Biology Program, and* [@]*Comprehensive Cancer Center, The Ohio State University, Columbus, Ohio 43210*

Received March 28, 2009; Revised Manuscript Received May 19, 2009

ABSTRACT: Transient-state kinetic techniques were used to resolve the kinetic mechanism of DNA polymerization catalyzed by an exonuclease-deficient mutant of *Sulfolobus solfataricus* P2 DNA polymerase B1 (PolB1 exo-). Here, we report the kinetic parameters of several elementary steps for the forward polymerization reaction. PolB1 exo- binds tightly to DNA (K_d^{DNA} = 1.8 nM) and a correct incoming nucleotide (apparent K_d^{dTTP} = 11 μM). Moreover, several lines of kinetic evidence suggested that correct nucleotide incorporation catalyzed by PolB1 exo- was limited by a protein conformational change which precedes the chemistry step. The utilization of an "induced fit" mechanism by PolB1 exo- was supported by the following: a small, α-thio elemental effect of 1.5, varying DNA dissociation rates for the binary complex (0.043 s^{-1}) as well as ternary complexes before (0.18 s^{-1}) and after (0.0071 s^{-1}) a conformational change, a greater amplitude for the pulse−chase than the pulse−quench reaction, and an activation energy barrier of 38 kcal/mol which is greater than the predicted values of phosphodiester bond formation both in solution and within a polymerase active site. Lastly, PolB1 exo- exhibited a low processivity value of 15, thereby suggesting a protein cofactor confers this replicative DNA polymerase with higher processivity in vivo.

Elucidating the reaction pathway is an important goal toward understanding the catalytic events performed by an enzyme. To achieve this objective, a reaction pathway is established by identifying the chemical and conformational intermediates of each step and by measuring the rate and equilibrium constants for the elementary steps of converting substrate(s) into product(s). This knowledge subsequently provides the foundation for defining enzymatic specificity and the rate-limiting step. In pursuit of this goal, we have employed transient-state kinetic techniques to define the minimal kinetic mechanism of DNA polymerization catalyzed by an exonuclease-deficient mutant of *Sulfolobus solfataricus* P2 DNA polymerase B1 (PolB1 exo-).[1]

PolB1, a B-family DNA polymerase, is one of four DNA polymerases encoded within the *S. solfataricus* P2 genome: three B-family polymerases and one DNA lesion bypass Y-family polymerase, i.e., DNA polymerase IV (Dpo4) (*1*). Thus far, biochemical characterization of the isolated gene products has deemed only two of these polymerases functional in vitro: PolB1 and Dpo4 (*2*−*4*). Furthermore, a direct physical interaction between PolB1 and Dpo4 has been demonstrated (*3*), and surprisingly, protein levels are similar for both polymerases during normal growth conditions (*5*).

Although a myriad of DNA polymerases have been biochemically characterized, detailed kinetic mechanisms of their 5′→3′ polymerase activity have been established for only a handful of DNA polymerases. Some of the more prominent examples include *Escherichia coli* DNA polymerase I (*6*−*11*), bacteriophage T7 DNA polymerase (T7 DNA Pol) (*12*−*14*), human immunodeficiency virus type I reverse transcriptase (HIV-1 RT) (*15*−*17*), bacteriophage T4 DNA polymerase (T4 DNA Pol) (*10*, *18*−*22*), *Saccharomyces cerevisiae* DNA polymerase η (*23*), and *S. solfataricus* P2 Dpo4 (*24*−*26*). Of these and others, T4 DNA polymerase is the only B-family member to have undergone rigorous kinetic studies. Herein, we report the first kinetic mechanism of an archaeal B-family polymerase. *S. solfataricus* P2 PolB1 was selected for several reasons. (i) The crystal structure for *S. solfataricus* MT4 PolB1, in which the amino acid sequence differs from strain P2 by only two residues, has been determined (*27*). (ii) It is an ideal model system for DNA replication because the replication machinery is a simplified version of that in eukaryotes (see ref (*28*) for a review). (iii) The kinetic mechanism of Dpo4 has been studied in detail

[†]This work was supported by a National Science Foundation Career Award to Z.S. (Grant MCB-0447899). J.A.B. was supported by the National Institutes of Health Chemistry and Biology Interface Program at The Ohio State University (Grant 5 T32 GM008512-11).

*To whom correspondence should be addressed: 880 Biological Sciences, 484 W. 12th Ave., Columbus, OH 43210. Telephone: (614) 688-3706. Fax: (614) 292-6773. E-mail: suo.3@osu.edu.

[1]Abbreviations: BSA, bovine serum albumin; ddTTP, 2′,3′-dideoxythymidine 5′-triphosphate; dNTP, 2′-deoxynucleoside 5′-triphosphate; Dpo4, DNA polymerase IV; DTT, dithiothreitol; EDTA, ethylenediaminetetraacetic acid; HIV-1 RT, human immunodeficiency virus type 1 reverse transcriptase; PCNA, proliferating cell nuclear antigen; PolB1, DNA polymerase B1; PolB1 exo-, exonuclease-deficient DNA polymerase B1; Sp-dNTPαS, S_p isomer of 2′-deoxynucleoside 5′-*O*-(1-thiotriphosphate); *Sso*, *Sulfolobus solfataricus*; T4 DNA Pol, T4 DNA polymerase; TLS, translesion DNA synthesis.

 Published on Web 05/20/2009 © 2009 American Chemical Society

which could facilitate future studies of the mechanism of polymerase switching between PolB1 and Dpo4 (*25*, *26*). (iv) Biochemical data are available for interactions among PolB1, Dpo4, and accessory proteins (*3*, *29*−*31*). (v) In our preceding paper (*32*), we showed that the polymerase active site confers a fidelity of 10^{-4} to 10^{-6} while the exonuclease active site increases the fidelity by 14-fold for an overall fidelity of 10^{-6} to 10^{-8} at pH 6.0 (*32*). Using an exonuclease-deficient mutant of PolB1, we have dissected the minimal kinetic pathway for DNA polymerization by measuring the elementary steps in a single catalytic cycle. Surprisingly, several of the reported parameters are similar to those of Dpo4, and we provide kinetic evidence that PolB1, like Dpo4, utilizes an induced fit mechanism during correct nucleotide incorporation.

EXPERIMENTAL PROCEDURES

Materials. These chemicals were purchased from the following companies: [α-^{32}P]dTTP, MP Biomedicals (Solon, OH); [γ-^{32}P]ATP, PerkinElmer (Boston, MA); Biospin columns, Bio-Rad Laboratories (Herclues, CA); dNTPs, GE Healthcare (Piscataway, NJ); OptiKinase, USB (Cleveland, OH); Sp-dTTPαS and Sp-dGTPαS, Biolog-Life Science Institute (Bremen, Germany); ddTTP, Trilink Biotechnologies (San Diego, CA).

Pre-Steady-State Kinetic Assays. *S. solfataricus* PolB1 exo- (D231A/E233A/D318A) fused to a C-terminal His_6 tag was overexpressed in *E. coli* and purified as described previously (*32*). The D-1 DNA substrate shown in Figure 1 was prepared as described previously (*24*, *32*). All experiments using PolB1 exo- were performed at 37 °C, if not specified, and in optimized reaction buffer A which contained 50 mM HEPES (pH 7.5), 15 mM $MgCl_2$, 75 mM NaCl, 5 mM DTT, 10% glycerol, and 0.1 mg/mL BSA (*32*). Please note that, although the PolB1 enzyme utilized in these studies is an exonuclease-deficient mutant, PolB1 exo- was never pre-incubated in the presence of magnesium. As in the case of HIV-1 RT, the kinetic results may be slightly different when the enzyme is incubated with or without magnesium (*16*). Fast reactions were conducted at 37 °C using a rapid chemical-quench flow apparatus (KinTek). All reported concentrations are the final reaction values.

Active Site Titration Assay. The equilibrium dissociation constant (K_d^{DNA}) of the binary complex was determined by mixing a pre-incubated solution of PolB1 exo- (45 nM) and increasing concentrations of 5′-radiolabeled D-1 DNA (2.5−100 nM) with dTTP (100 μM). All reactions were quenched at 1.8 s (equivalent to eight half-times, $t_{1/2}$) to achieve the maximal first-turnover amplitude.

Measurement of the Phosphorothioate Elemental Effect. A pre-incubated solution of PolB1 exo- (120 nM) and 5′-radiolabeled 21/41-mer D-1 (30 nM) was rapidly mixed with either dTTP (100 μM) or Sp-dTTPαS (100 μM, >95% purity) in buffer A and the reaction terminated with 0.37 M EDTA. For incorporation of an incorrect nucleotide, the reaction was initiated with either dGTP (500 μM) or Sp-dGTPαS (500 μM, >95% purity). The S_p isomers were used, as opposed to the R_p isomers, because of the stereoselectivity observed previously (*33*, *34*).

Pulse−*Chase and Pulse*−*Quench Experiments*. Pulse−chase and pulse−quench experiments were performed in buffer A using a rapid chemical-quench flow instrument. A pre-incubated solution containing PolB1 exo- (100 nM) and unlabeled D-1 DNA substrate (100 nM) was loaded into one sample loop and rapidly mixed with buffer containing [α-^{32}P]dTTP (50 μM) from a second sample loop for reaction times ranging from 22 ms to 2.0 s. In the pulse−quench experiment, reactions were immediately quenched with 1 M HCl. In the pulse−chase experiment, reactions were immediately chased with 1.0 mM unlabeled dTTP for 30 s, followed by quenching with 1 M HCl. In both cases, quenched reaction mixtures were treated with chloroform and neutralized with 1 M NaOH.

Product Analysis. Reaction products were analyzed by sequencing gel electrophoresis (17% acrylamide, 8 M urea, and 1× TBE running buffer) and quantitated using a Typhoon TRIO (GE Healthcare) and ImageQuant (Molecular Dynamics). For the pulse−chase and pulse−quench assays, DNA products were resolved using a 20% highly cross-linked polyacrylamide gel matrix as described previously (*35*).

Data Analysis. Data were fit by nonlinear regression using KaleidaGraph (Synergy Software).

Data from the burst and pulse−chase experiments were fit to eq 1

$$[\text{product}] = A[1 - \exp(-k_1 t) + k_2 t] \quad (1)$$

where A is the fraction of active enzyme, k_1 is the observed burst rate, and k_2 is the observed steady-state rate.

Data from the experiments performed under steady-state conditions were fit to eq 2

$$[\text{product}] = k_{ss} E_0 t + E_0 \quad (2)$$

where k_{ss} is the steady-state rate constant of dNTP incorporation at the initial active enzyme concentration of E_0.

Data from the assay measuring the DNA dissociation rate of the binary complex were fit to eq 3

$$[\text{product}] = A[\exp(-k_1 t)] + C \quad (3)$$

where A is the reaction amplitude, k_1 is the observed rate constant, and C is the ^{32}P-labeled product concentration in the presence of a DNA trap for unlimited time.

For the active site titration assay, the resulting product concentration (equivalent to burst amplitude) was plotted versus the concentration of D-1 DNA and fit via quadratic regression to eq 4

$$[\text{E}\cdot\text{DNA}] = 0.5(K_d^{DNA} + E_0 + D_0) - 0.5[(K_d^{DNA} + E_0 + D_0)^2 - 4E_0D_0]^{1/2} \quad (4)$$

where K_d^{DNA} represents the equilibrium dissociation constant for the binary complex (E·DNA), E_0 is the active enzyme concentration, and D_0 is the DNA concentration.

Data from the experiments performed under single-turnover conditions were fit to eq 5

$$[\text{product}] = A[1 - \exp(-k_{obs} t)] \quad (5)$$

where A is the reaction amplitude and k_{obs} is the observed single-turnover rate.

When the assumption $k_1 \gg k_2$ is not valid for burst experimental data (refer to eq 1), eq 6 was applied.

$$[\text{product}] = A\{(k_1k_2/k_1 + k_2)t + (k_1/k_1 + k_2)^2[1 - \exp(-k_1 + k_2)t]\} \quad (6)$$

Using k_p and temperature data from ref (*32*), the activation energy was determined using the Arrhenius equation

$$k_p = A_r[\exp(-E_a/RT)] \quad (7)$$

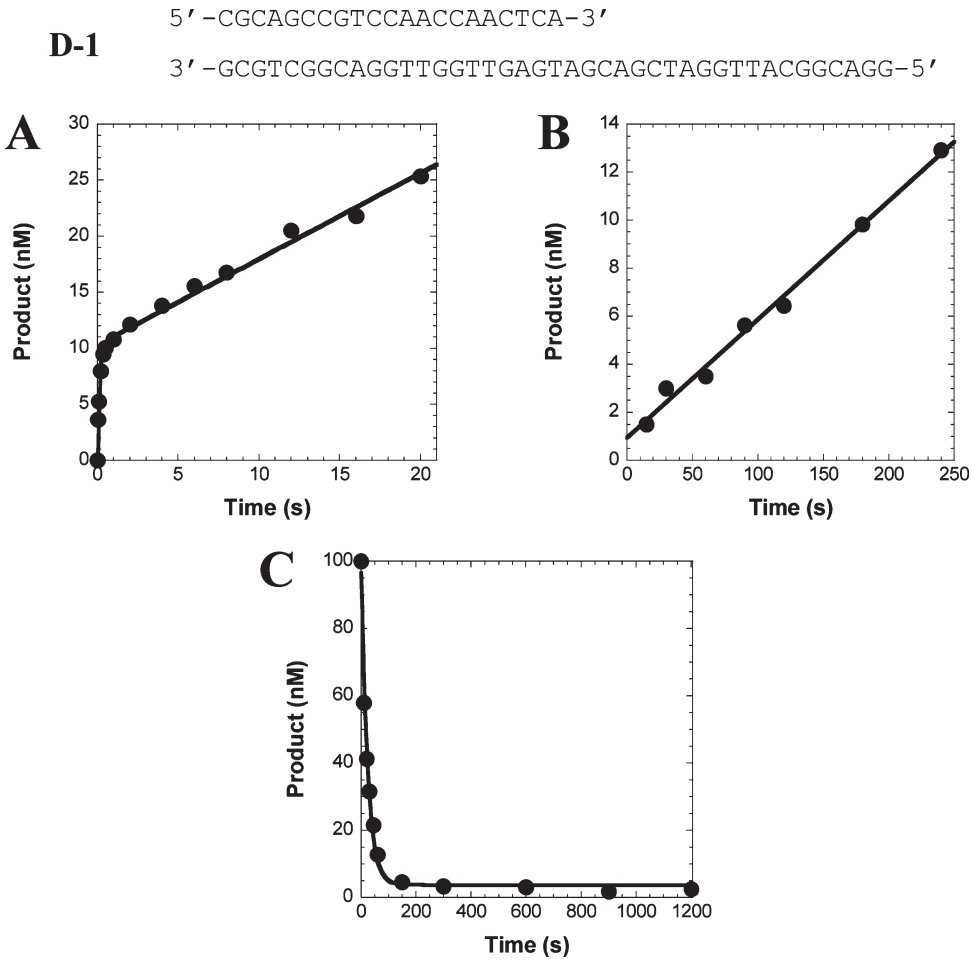

FIGURE 1: Pre-steady-state and steady-state kinetics of incorporation of dTTP into D-1 DNA by PolB1 exo-. (A) A pre-incubated solution of PolB1 exo- (30 nM) and 5′-^{32}P-labeled D-1 DNA (120 nM) was rapidly mixed with dTTP (100 μM) and the reaction quenched at various times with 0.37 M EDTA. The data were fit by nonlinear regression to a biphasic equation (eq 1, Experimental Procedures) with an observed burst and steady-state rate of 9 ± 1 and 0.074 ± 0.05 s^{-1}, respectively. (B) Incorporation of dTTP into D-1 was independently measured under steady-state conditions, whereby the addition of 100 μM dTTP with a pre-equilibrated solution of PolB1 exo- (1 nM) and 5′-^{32}P-labeled D-1 DNA (250 nM) initiated the reaction. At various times, the reaction was terminated using 0.37 M EDTA. The data were fit to a linear relationship (eq 2, Experimental Procedures) which yielded a steady-state rate constant of 0.038 s^{-1}. (C) The DNA dissociation rate constant from the binary complex was measured by mixing a pre-equilibrated solution of PolB1 exo- (50 nM) and 5′-^{32}P-labeled D-1 DNA (100 nM) with unlabeled D-1 DNA (2.5 μM) for various time intervals. Then, dTTP (133 μM) was added for 15 s before the reaction was quenched. Data were fit to a single-exponential equation (eq 3, Experimental Procedures) to yield a rate constant of 0.043 ± 0.003 s^{-1}.

where k_p is the maximum rate of nucleotide incorporation, A_r is the proportionality constant, E_a is the activation energy, R is the universal gas constant, and T is the reaction temperature in kelvin.

Data from the processive elongation of 21/41-mer to 27/41-mer were modeled using an improved personal computer version of Kinsim provided by C. Frieden (Washington University, St. Louis, MO) (*36*). Final fitting of the data was accomplished by nonlinear regression using an improved personal computer version of Fitsim (*37*).

RESULTS

Biphasic Kinetics Observed for PolB1 exo-. To begin characterizing *S. solfataricus* P2 PolB1 exo-, we first performed a burst experiment at 37 °C. The rationalization for studying PolB1 exo- at a suboptimal temperature of 37 °C was explained in our preceding paper (*32*). Results from a burst assay can yield insight into (i) the rate of nucleotide incorporation occurring at the enzyme's active site during the first turnover and (ii) whether product release from the enzyme during subsequent turnovers is rate-limiting. A pre-incubated solution of PolB1 exo- (30 nM based on UV absorbance measurements) and radiolabeled D-1 DNA (120 nM) was rapidly mixed with dTTP (100 μM) and the reaction quenched with EDTA at various reaction times. The time course of product formation indicated that PolB1 exo- followed biphasic or "burst" kinetics (Figure 1A). Applying eq 1 (Experimental Procedures) to the plot resolved an observed burst rate of 9 ± 1 s^{-1} (exponential phase) and an observed linear-phase rate of 0.074 ± 0.05 s^{-1}. As observed with Dpo4 (*25*), the burst phase was likely limited by nucleotide incorporation in the first turnover while the linear phase could be the steady-state phase of product formation during subsequent enzyme turnovers (Scheme 1). To evaluate this possibility, we performed the following steady-state kinetic assay: PolB1 exo- (1 nM) was pre-equilibrated with a large excess of substrate (i.e., 250 nM radiolabeled D-1 DNA) prior to initiation of the reaction with dTTP (100 μM). A plot of product concentration versus time (Figure 1B) was linear and was fit to eq 2 (Experimental Procedures) which yielded a steady-state rate of 0.038 s^{-1}. This value was within 2-fold of 0.074 ± 0.05 s^{-1} determined in Figure 1A, thereby confirming that the linear phase under burst

Scheme 1

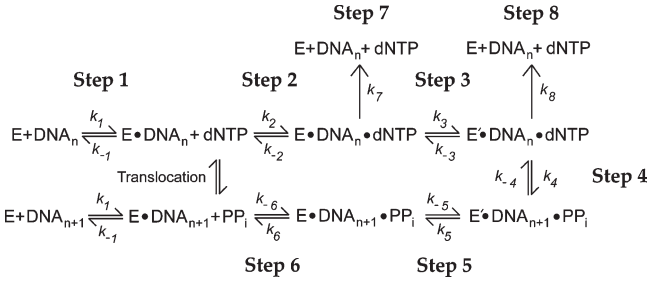

conditions was indeed a steady-state phase. In this phase, production formation is usually limited by the slow dissociation of the binary complex (E·DNA). To confirm this kinetic trend, we directly measured the DNA dissociation rate. PolB1 exo- (50 nM) was pre-incubated with 5′-radiolabeled D-1 DNA (100 nM) and mixed with an excess of unlabeled D-1 DNA (2.5 μM) from 10 s to 20 min. Then, dTTP (133 μM) was added for 15 s so that any DNA substrate in complex with PolB1 exo- could be extended. The concentration of the radioactive DNA product was plotted versus time and fit to a single-exponential equation (eq 3) (Figure 1C). The measured rate of 0.043 ± 0.003 s^{-1} (k_{-1} in Scheme 1) was similar to the rates of 0.038 and 0.074 s^{-1} determined in panels A and B of Figure 1, substantiating the observation that multiple enzyme turnovers were limited by the dissociation of the E·DNA complex.

Active Site Titration. Since PolB1 exo- exhibited burst kinetics, this implied a stable binary complex facilitated the rapid incorporation of dTTP so that the equilibrium dissociation constant (K_d^{DNA}) of the binary complex can be measured by titrating the active site of PolB1 exo- with varying concentrations of DNA. We conducted this active site titration assay by pre-incubating PolB1 exo- (45 nM based on UV absorbance measurements) with increasing concentrations of 5′-radiolabeled D-1 DNA (2.5−100 nM), starting the reaction by adding dTTP (100 μM), and quenching all reactions at 1.8 s with EDTA. For each DNA concentration, the reaction was performed in triplicate. The average product concentration was plotted for each concentration of DNA (Figure 2) and fit to a quadratic equation (eq 4). A K_d^{DNA} of 1.8 ± 0.4 nM and an E_0 of 18.9 ± 0.4 nM were extracted. This E_0 equates to 42% enzyme activity which is similar to that determined for HIV-1 RT (*15*). Henceforth, all experiments described below were performed using the active site enzyme concentration. Lastly, the apparent second-order binding rate constant (k_1 in Scheme 1) of the binary complex can be calculated by substituting the measured values for k_{-1} and K_d^{DNA} into the following equation: $k_1 = k_{-1}/K_d^{DNA} = (0.043\ s^{-1})/(1.8 \times 10^{-9}\ M) = 2.4 \times 10^7\ M^{-1}\ s^{-1} = 24\ \mu M^{-1}\ s^{-1}$.

Rates of Association and Dissociation of an Incoming Nucleotide. In the accompanying paper (*32*), we measured the apparent equilibrium dissociation constant ($K_d^{dNTP} = 11 \pm 2\ \mu$M) and maximum rate ($k_p = 8.2 \pm 0.6$ s^{-1}) of dTTP incorporation into D-1 DNA catalyzed by PolB1 exo- under single-turnover conditions. Assuming the association rate (k_2 in Scheme 1) of dTTP, a small molecule, approaches the diffusion limit of 1.0×10^8 M^{-1} s^{-1}, we estimated the upper limit of the dTTP dissociation rate to be 1100 s^{-1} ($k_{-2} = k_2 K_d^{dNTP}$) which is too fast to be accurately measured by current transient kinetic techniques.

PolB1 exo- Exhibited Low Processivity. For a DNA polymerase, the term processivity describes the number of nucleotides incorporated per DNA binding event, and this can

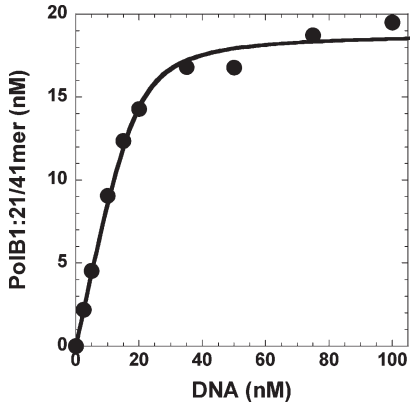

FIGURE 2: Active site titration of PolB1 exo-. PolB1 exo- (45 nM) and increasing concentrations of 5′-radiolabeled D-1 DNA (2.5−150 nM) were mixed with dTTP (100 μM). All reactions were quenched at 1.8 s using EDTA. The product concentration was plotted as a function of substrate concentration and fit to eq 4 (Experimental Procedures). An equilibrium dissociation constant of 1.8 ± 0.4 nM and an active enzyme concentration of 18.9 ± 0.4 nM were measured.

be quantitatively defined as the ratio of the polymerization rate divided by the DNA dissociation rate. To kinetically investigate the processivity of PolB1 exo-, a pre-incubated solution of PolB1 exo- (35 nM) and 5′-radiolabeled D-1 DNA (100 nM) were rapidly mixed with dCTP, dGTP, and dTTP (100 μM each) in reaction buffer A before the reaction was quenched with EDTA after 8 ms to 1.75 s. These reaction conditions allowed PolB1 to elongate 21/41-mer to 27/41-mer in a single binding event, since the DNA substrate was in molar excess over the enzyme. Each DNA species was resolved using polyacrylamide gel electrophoresis and quantitated using ImageQuant (Figure 3A). Then, the computer simulation programs Kinsim (*36*) and Fitsim (*37*) were used to fit the data to a mechanism considering six consecutive nucleotide incorporations and seven DNA dissociation rates for the possible binary complexes in the reaction pathway (Figure 1 of the Supporting Information). Fitsim generated the following rates of polymerization for the formation of each designated product: 4.8 ± 0.2 s^{-1} for 22-mer, 7.5 ± 0.5 s^{-1} for 23-mer, 12 ± 1 s^{-1} for 24-mer, 8.2 ± 0.8 s^{-1} for 25-mer, 4.9 ± 0.4 s^{-1} for 26-mer, and 15 ± 3 s^{-1} for 27-mer (Figure 3B). Meanwhile, the rates of DNA dissociation were 0.6 ± 0.1 s^{-1} for E·21/41-mer, 0.7 ± 0.1 s^{-1} for E·22/41-mer, 0.7 ± 0.2 s^{-1} for E·23/41-mer, 0.4 ± 0.2 s^{-1} for E·24/41-mer, 0.2 ± 0.1 s^{-1} for E·25/41-mer, 0.7 ± 0.5 s^{-1} for E·26/41-mer, and 0.8 ± 0.2 s^{-1} for E·27/41-mer. These DNA dissociation rates (0.2−0.8 s^{-1}) are greater than the dissociation rates (~0.043 s^{-1}) of the PolB1 exo-·DNA complex measured in Figure 1 which suggested that DNA rapidly dissociated from an unidentified intermediate during processive synthesis. Using the average rate of polymerization (8.7 s^{-1}) and DNA dissociation (0.6 s^{-1}), the processivity of PolB1 exo- was calculated to be 15.

Elemental Effect of Nucleotide Incorporation. The presence of a burst (Figure 1A) suggested that the rate of the first turnover is limited by the chemistry step (step 4 in Scheme 1), a protein conformational change preceding chemistry (step 3 in Scheme 1), or a combination of these two steps. To discern the rate-limiting step of correct nucleotide incorporation, the observed rate constants for the incorporations of dTTP and Sp-dTTPαS, an analogue with a phosphothioate group at the α-phosphate position, were measured under single-turnover conditions. PolB1 exo- (120 nM) and 5′-^{32}P-labeled D-1

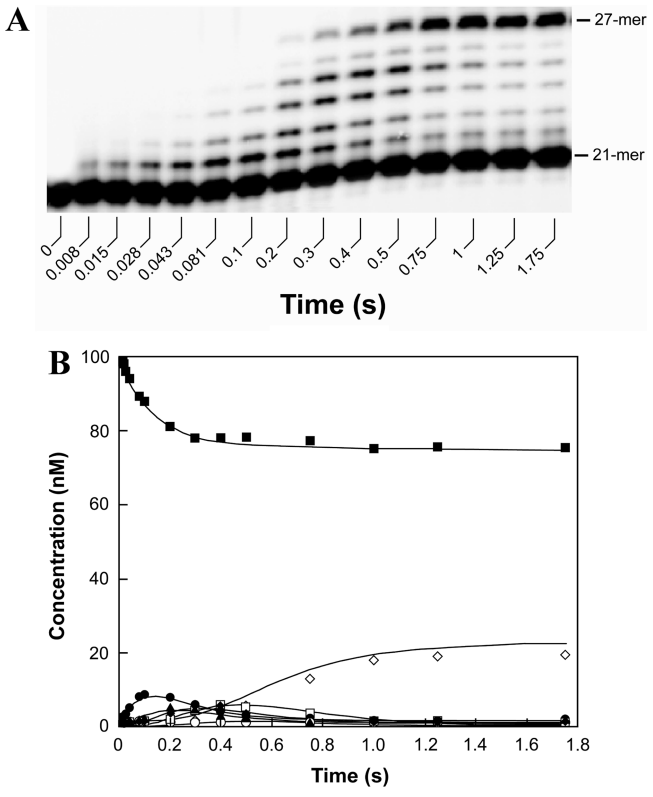

FIGURE 3: PolB1 exo- exhibited low processivity. A pre-incubated solution of PolB1 exo- (35 nM) and 5′-radiolabeled D-1 DNA (100 nM) was reacted with dCTP, dGTP, and dTTP (200 μM each) for various times until the reaction was quenched with 0.37 M EDTA. Products were analyzed using sequencing gel analysis, and the gel image is shown in panel A. (B) The amounts of remaining substrate [21-mer (■)] and each product [22-mer (●), 23-mer (▲), 24-mer (◆), 25-mer (□), 26-mer (○), and 27-mer (◇)] were plotted as a function of time. The solid lines represent the best fits generated by computer simulation using a mechanism that defines the rates for six consecutive nucleotide incorporations and seven DNA dissociations from the possible PolB1·DNA species. The rates of polymerization for the formation of each product were 4.8 ± 0.2 s^{-1} for 22-mer, 7.5 ± 0.5 s^{-1} for 23-mer, 12 ± 1 s^{-1} for 24-mer, 8.2 ± 0.8 s^{-1} for 25-mer, 4.9 ± 0.4 s^{-1} for 26-mer, and 15 ± 3 s^{-1} for 27-mer, while the rates of DNA dissociation were 0.6 ± 0.1 s^{-1} for E·21/41-mer, 0.7 ± 0.1 s^{-1} for E·22/41-mer, 0.7 ± 0.2 s^{-1} for E·23/41-mer, 0.4 ± 0.2 s^{-1} for E·24/41-mer, 0.2 ± 0.1 s^{-1} for E·25/41-mer, 0.7 ± 0.5 s^{-1} for E·26/41-mer, and 0.8 ± 0.2 s^{-1} for E·27/41-mer.

DNA (30 nM) were mixed with 100 μM dTTP or Sp-dTTPαS in independent reaction mixtures. After the curves in Figure 4A had been fit to a single-exponential equation (eq 5), the extracted k_{obs} values were 10.3 ± 0.6 and 7.0 ± 0.4 s^{-1} for dTTP and Sp-dTTPαS, respectively. Thus, the elemental effect, a ratio of $k_{obs,dTTP}/k_{obs,Sp\text{-}dTTP\alpha S}$, was calculated to be 1.5. Previously, an elemental effect of 4−11 has been considered evidence of a rate-limiting chemistry step (*38*); therefore, these results suggested that correct nucleotide incorporation may not be limited by the rate of phosphodiester bond formation (step 4).

Next, we performed an analogous experiment to deduce the rate-limiting step of incorrect nucleotide incorporation. For the incorporation of dGTP or Sp-dGTPαS (500 μM) into the same D-1 DNA substrate, the respective observed rate constants were 0.010 ± 0.001 and 0.00028 ± 0.00002 s^{-1} which translated into an α-thio elemental effect of 36 (Figure 4B). Relative to what was observed with correct dTTP, this larger elemental effect suggested that phosphodiester bond formation may be partially rate-limiting.

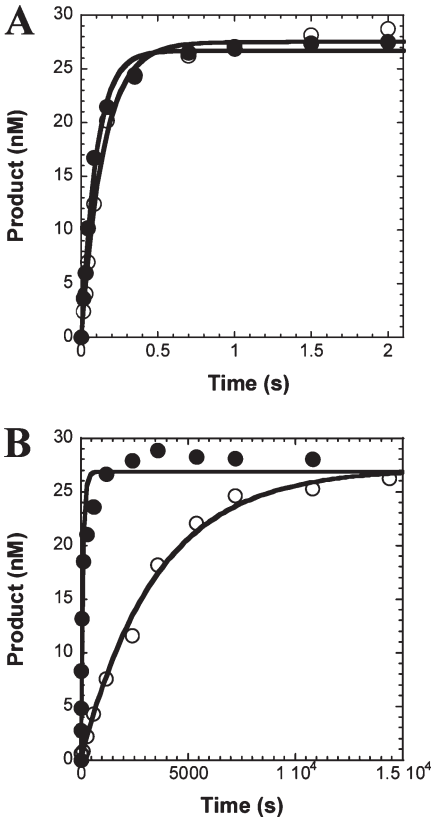

FIGURE 4: Elemental effect on the rate of correct and incorrect nucleotide incorporation. PolB1 exo- (120 nM) and 5′-^{32}P-labeled D-1 DNA (30 nM) were rapidly mixed with (A) 100 μM dTTP (●) or Sp-dTTPαS (○) in parallel time courses. The data were fit to a single-exponential equation (eq 5, Experimental Procedures) to extract k_{obs} values of 10.3 ± 0.6 and 7.0 ± 0.4 s^{-1} for dTTP and Sp-dTTPαS, respectively, for a calculated elemental effect of 1.5. (B) The same PolB1·D-1 solution was mixed with 500 μM dGTP (●) or Sp-dGTPαS (○) in parallel time courses. The data were fit to a single-exponential equation (eq 5, Experimental Procedures) to extract k_{obs} values of 0.010 ± 0.001 and 0.00028 ± 0.00002 s^{-1} for dGTP and Sp-dGTPαS, respectively, for a calculated elemental effect of 36.

Determination of the Rate of Dissociation from the E·DNA·dNTP Complex. Following formation of the E·DNA·dNTP complex, DNA can either dissociate (step 7 in Scheme 1) or continue along the reaction pathway as part of a ternary species which undergoes a protein conformational change (step 3 in Scheme 1) leading to the formation of the E′·DNA·dNTP complex. To assess the former possibility, the DNA dissociation rate (k_7) of the E·DNA·dNTP complex was measured by reacting a pre-incubated solution of PolB1 exo- (55 nM) and 5′-^{32}P-labeled D-1 DNA (60 nM) with Sp-dTTPαS (100 μM) in the absence or presence of an unlabeled DNA trap (2.5 μM D-1 DNA) at 37 °C. Please note that, rather than dTTP, Sp-dTTPαS was used since it is incorporated at a slower rate (Figure 4A). This will enhance the kinetic partitioning from the E·DNA·dNTP complex to E, DNA, and dNTP. Also, the purpose of the DNA trap is to sequester any of the PolB1 exo- molecules that dissociate (step 7 of Scheme 1) so that the reverse reaction is attenuated. After the data points had been fit to eq 1, identical burst rates of 7.8 ± 0.4 s^{-1} were determined, although the burst amplitudes were 43.3 ± 0.5 and 42.3 ± 0.5 nM in the absence and presence of the DNA trap, respectively (Figure 5). The amplitude difference increased (~7 nM) when the reaction was performed at a lower temperature of 35 °C which enhanced partitioning from the E·DNA·dNTP complex to E, DNA, and

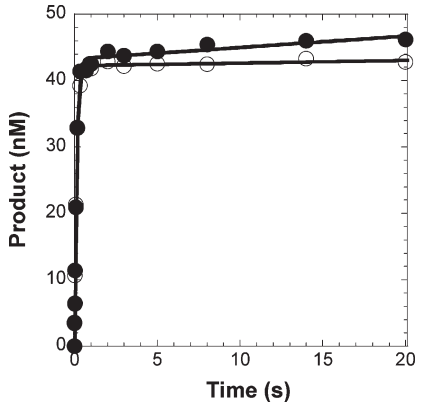

FIGURE 5: Measurement of the dissociation rate for the E·DNA·dNTP complex. PolB1 exo- (55 nM) and 5′-^{32}P-labeled D-1 DNA (60 nM) were rapidly mixed with 100 μM Sp-dTTPαS in the absence (●) or presence (○) of an unlabeled DNA trap (2.5 μM D-1). An identical burst rate of 7.8 ± 0.4 s^{-1} was determined for both time courses, while the burst amplitudes were 43.3 ± 0.5 and 42.3 ± 0.5 nM in the absence and presence of the DNA trap, respectively. Thus, an amplitude reduction of 2.3% equates to a k_7 of 0.18 ± 0.1 s^{-1}.

dNTP (Figure 2 of the Supporting Information). The kinetic parameter k_7 was estimated from the following relationship: $A_{trap}/A_{no\ trap} = k_{obs}/(k_{obs} + k_7) = 42.3/43.3 = 7.8\ s^{-1}/(7.8\ s^{-1} + k_7)$. Solving this equation yielded a DNA dissociation rate of 0.18 ± 0.01 s^{-1} for the E·DNA·dNTP complex at 37 °C. This result suggested that dissociation of DNA from the ternary complex (step 7 in Scheme 1, k_7) is faster relative to the dissociation of the binary complex (step 1 in Scheme 1, k_{-1}). Interestingly, the value of k_7 at 37 °C is similar to the lower limit of the dissociation rates (0.2−0.8 s^{-1}) determined from the global fitting analysis (Figure 3), while the value of k_7 at 35 °C is similar to the upper limit (Figure 2 of the Supporting Information). Thus, the unidentified intermediate during processive polymerization in Figure 3 is likely to be the E·DNA·dNTP complex.

Measurement of the DNA Dissociation Rate of the E′·DNA·dNTP Complex. To determine k_8, a steady-state kinetic assay was employed, whereby a pre-incubated solution of PolB1 exo- (1 nM) and 5′-^{32}P-labeled D-1 DNA (250 nM) was rapidly mixed with ddTTP (100 μM) in the absence or presence of dCTP (100 μM), the next correct nucleotide. For the former reaction (i.e., without dCTP), the steady-state rate should correspond to the rate of dissociation of DNA from the binary complex as measured in Figure 1. For the latter reaction (i.e., with dCTP), PolB1 exo- should extend D-1 DNA by first incorporating ddTTP (PolB1 exo-·DNA_{n+1}) and then form a ternary complex with dCTP for the second correct incorporation during the first enzyme binding event. However, because of the initially incorporated ddTMP which lacks the 3′-OH group, the second incorporation can only proceed up to step 3 in Scheme 1. Thus, following ddTTP incorporation, PolB1 exo- has to dissociate from the E′·DNA_{n+1}·dCTP complex and then bind to other DNA molecules. Moreover, the multiple-turnover rate in the presence of dCTP is limited by the off rate of DNA from the E′·DNA_{n+1}·dCTP complex. The data points for both reactions were fit to eq 2 (Experimental Procedures), and the steady-state rates were 0.029 and 0.0071 s^{-1} in the absence and presence of dCTP, respectively (Figure 6A). These steady-state rates differed by 4.1-fold, thereby indicating that (i) the presence of the next correct nucleotide inhibited DNA dissociation and (ii) a tightly bound ternary complex (E′·DNA_{n+1}·dCTP) was formed.

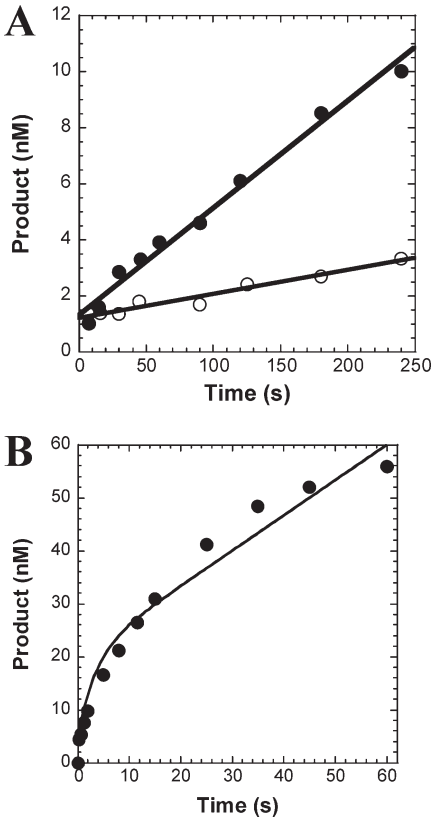

FIGURE 6: Measurement of the dissociation rate for the E′·DNA·dNTP complex. (A) PolB1 exo- (1 nM) and 5′-^{32}P-labeled D-1 DNA (250 nM) was rapidly mixed with 100 μM ddTTP in the absence (●) or presence (○) of the next correct nucleotide (100 μM dCTP). Fitting the data to eq 2 (Experimental Procedures) generated steady-state rates of 0.029 and 0.0071 s^{-1} in the absence and presence of dCTP, respectively. (B) A pre-incubated solution of PolB1 exo- (30 nM) and 5′-^{32}P-labeled D-1 DNA (120 nM) was rapidly mixed with 100 μM ddTTP. Data were fit to eq 6 (Experimental Procedures) which yielded an observed burst and steady-state rate of 0.3 ± 0.2 and 0.04 ± 0.01 s^{-1}, respectively.

Since ddTTP was used for the assay described above, it is possible that the steady-state rate measured using ddTTP may not be limited by the dissociation of the product from the enzyme. To validate the steady-state rate of 0.029 s^{-1} measured above, a burst experiment was performed with ddTTP under reaction conditions identical to those described in the legend of Figure 1A. The biphasic curve was fit to eq 6 (Experimental Procedures) which yielded an observed burst and steady-state rate of 0.3 ± 0.2 and 0.04 ± 0.01 s^{-1}, respectively (Figure 6B). The similar steady-state rates of 0.029 and 0.04 ± 0.01 s^{-1} obtained under steady-state and burst conditions, respectively, confirmed that these rates were limited by dissociation of DNA from the E·DNA binary complex.

Pulse−Chase and Pulse−Quench Experiments. Pulse−chase and pulse−quench experiments were performed to further validate the occurrence of a conformational step (step 3) preceding the chemistry step (step 4). For this assay, a pre-incubated solution of PolB1 exo- (100 nM) and unlabeled D-1 DNA (100 nM) was rapidly mixed with [α-^{32}P]dTTP (50 μM). The pulse−quench reactions were immediately quenched with 1 M HCl, and the mixtures were denatured with chloroform and neutralized with 1 M NaOH. In contrast, the pulse−chase reactions were chased using an excess of unlabeled dTTP (1 mM) for 30 s prior to the initiation of the quenching, denaturation, and

neutralization steps. During the chase time period, the PolB1 exo-·D-1·[α-^{32}P]dTTP complexes, which were partitioning between both forward and reverse directions, would be chased in the forward direction to form more radiolabeled products. If more product formation occurs during the pulse−chase reaction, then this implies that (i) a ternary complex intermediate, which is distinguishable from the ground-state ternary complex PolB1 exo-·D-1·[α-^{32}P]dTTP, occurred along the reaction pathway and (ii) the chemistry step (step 4 in Scheme 1) is flanked immediately before and after by slower steps (steps 3 and 5, respectively, in Scheme 1). Equation 1 was applied to the time courses, and amplitudes of 75 ± 3 and 61 ± 2 nM for the pulse−chase and pulse−quench assays, respectively, were determined (Figure 7). This amplitude difference of 14 nM (~19%) provided evidence for the existence of a stably bound ternary complex that accumulated prior to the chemical reaction. Since nucleotide binding was rapid for PolB1 exo-, partitioning in the forward direction likely represented an accumulation of the E′·DNA·dNTP complex. Similar to what we have discussed in the kinetic studies of Dpo4 (*39*), the accumulated intermediate cannot be either E·DNA·dNTP or E·DNA.

Activation Energy Barrier for Nucleotide Incorporation. The Arrhenius activation energy (E_a) is the minimum amount of energy required for reactants to be converted into products during a chemical reaction. To determine the E_a required for PolB1 exo- to elongate a DNA substrate during a single nucleotide incorporation, we determined the k_p values of both correct and incorrect dNTP incorporations at various temperatures [Table 3 in our accompanying paper (*32*)]. These k_p values were then used to construct an Arrhenius plot [ln(k_p) vs temperature (1000/T)] which was subsequently fit to eq 7 (Experimental Procedures). This generated an E_a of 38 ± 3 kcal/mol for correct dTTP incorporation and an E_a of 55 ± 3 kcal/mol for incorrect dATP incorporation (Figure 8). Thus, 17 kcal/mol of additional energy is required for PolB1 exo- to catalyze a misincorporation.

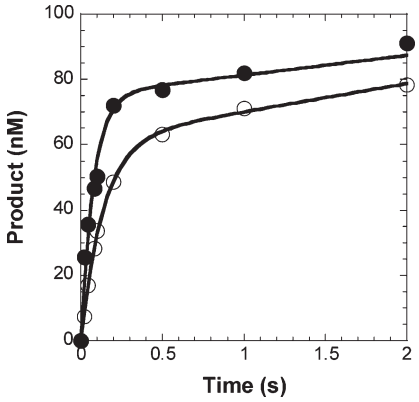

FIGURE 7: Pulse−chase and pulse−quench experiment. A pre-incubated solution of PolB1 exo- (100 nM) and unlabeled D-1 DNA (100 nM) was rapidly mixed with 50 μM [α-^{32}P]dTTP. The pulse−quench (○) reactions were immediately quenched with HCl (1 M), while the pulse−chase (●) reactions were chased with 1.0 mM nonradioactive dTTP for 30 s prior to acid quenching. Fitting the data to eq 1 (Experimental Procedures) yielded amplitudes of 75 ± 3 and 61 ± 2 nM for the pulse−chase and pulse−quench reactions, respectively.

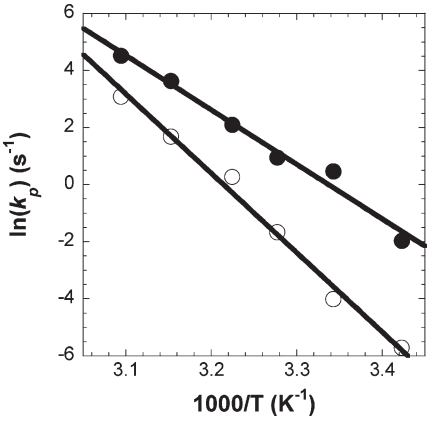

FIGURE 8: Activation energy for nucleotide incorporation. The k_p values (extracted from ref (*32*)) for dTTP (●) and dATP (○) were plotted as a function of reaction temperature and subsequently fit to eq 7 (Experimental Procedures). An activation energy of 38 ± 3 kcal/mol was determined for correct (dTTP·dA) nucleotide incorporation, while an activation energy of 55 ± 3 kcal/mol was determined for incorrect (dATP·dA) nucleotide incorporation.

DISCUSSION

Minimal Kinetic Mechanism for PolB1 exo-. The kinetic studies of several A-, B-, X-, and Y-family DNA polymerases reveal that these enzymes share a minimal kinetic mechanism of DNA synthesis shown in Scheme 1 (*40*). Our pre-steady-state kinetic analysis of PolB1 exo- suggested that this B-family member followed the same kinetic mechanism and binds substrates sequentially: DNA first followed by an incoming nucleotide. As indicated by the active site titration assay (Figure 2), PolB1 exo- binds to a 21/41-mer (primer−template) DNA substrate with a K_d^{DNA} value of 1.8 nM. The apparent ground-state binding affinity ($1/K_d^{dNTP}$) of an incoming nucleotide depended on whether a canonical base pair was formed. In general, the apparent binding affinity of a correct Watson−Crick base pair was ~1000-fold tighter than the weak apparent affinities of incorrect nucleotides [Table 2 in the accompanying paper (*32*)]. Furthermore, the kinetics of correct dTTP incorporation catalyzed by PolB1 exo- was biphasic (Figure 1A) which suggested that the first turnover was limited by either step 3, step 4, or both in Scheme 1 (see discussion below), while multiple turnovers were likely limited by dissociation of the elongated DNA product from the enzyme (step 1). The latter observation was corroborated by the fact that the steady-state turnover rate was similar to the dissociation rate of the PolB1·DNA complex (Figure 1). The existence of step 3 and its role as the rate-limiting step of correct nucleotide addition during the first turnover were supported by the following lines of kinetic evidence. (i) A small α-thio effect of 1.5 for the rate of dTTP incorporation relative to its α-thio analogue, dTTPαS (Figure 4A), suggested that the chemistry step (step 4) was unlikely the rate-limiting step. However, other evidence is required to support this conclusion because the intrinsic α-thio effect for any nucleotide incorporation is unknown, it is sensitive to the steric configuration at the α-phosphorus of a nucleotide bound at the active site of a polymerase, and it is influenced by the transition-state structure (*34*, *38*). (ii) Different DNA dissociation rates for k_{-1}, k_7, and k_8 (Figures 1, 5, and 6A) suggested the presence of E·DNA, E·DNA·dNTP, and E′·DNA·dNTP complexes, respectively, along the reaction pathway. (iii) A 14 nM (19%) higher reaction amplitude in the pulse−chase reaction over that observed in the pulse−quench reaction (Figure 7) suggested the existence of the E′·DNA·dNTP complex which did not yield products under pulse−quench reaction conditions but was chased to products by a large molar excess of dTTP under the pulse−chase conditions.

The accumulation of the E′·DNA·dNTP complex also suggested that step 5 is slow (*8*). Notably, the rates for steps 5 and 6 in Scheme 1 were not measured in this paper. (iv) An activation energy of 38 ± 3 kcal/mol for dTTP incorporation was determined from the dependence of ln k_p versus $1/T$ (Figure 8). This E_a value may represent the energy barrier for either step 3, step 4, or both because the k_p values are potentially limited by these steps. For uncatalyzed phosphodiester bond formation in solution, the E_a for its rate-limiting chemistry step is calculated to be 21.1 kcal/mol (*41*). If this reaction occurs at a polymerase active site, its E_a value should be significantly lower than 21.1 kcal/mol because enzymes are known to stabilize transition states and lower the activation energy barriers (*42*). Consistently, the activation energy barriers for the chemistry step of phosphodiester bond formation catalyzed by T7 DNA polymerase (*41*) and human DNA polymerase β (*43*) are predicted to be 12.3 and 17 kcal/mol, respectively. In comparison, our measured E_a value of dTTP incorporation was 21−25.7 kcal/mol greater than these predicted values and cannot represent the energy barrier for step 4. Thus, step 3 was the rate-limiting step of the first turnover during DNA synthesis catalyzed by PolB1 exo-.

Interestingly, the E_a for correct dTTP incorporation catalyzed by Dpo4 has been determined to be 32.9 kcal/mol and similarly used as one of the four lines of kinetic evidence to identify step 3 as the rate-limiting step (*25*, *26*). Previously, step 3 has also been recognized as the rate-limiting step for the kinetic mechanisms of correct nucleotide incorporation catalyzed by several other enzymes, including *E. coli* DNA polymerase I (*8*), T7 DNA polymerase (*12*, *14*), HIV-1 reverse transcriptase (*15*), and yeast DNA polymerase η (*44*). Although these enzymes share a rate-limiting protein conformational change, the exact physical nature of step 3 is unclear. Numerous X-ray crystallographic studies suggest that step 3 may reflect the open-to-close transition of the finger domain for the A-, B-, and X-family DNA polymerases (*45*−*49*). In contrast, nucleotide binding only induces the subtle repositioning of select active site residues of the X- and Y-family members (*50*, *51*). Recently, this assignment of the rate-limiting step has been further questioned due to fluorescence resonance energy transfer-based evidence for two A-family DNA polymerases, *E. coli* DNA polymerase I (*11*) and *Thermus aquaticus* DNA polymerase I (*52*), which show that the closure rate of the finger domain is too fast to limit catalysis. Thus, step 3 may correspond to the subtle repositioning of active site residues, substrates, and the network of water molecules in the active site pocket (*53*) prior to catalysis. This step may be more dramatic and difficult with high-fidelity PolB1 exo- than with error-prone Dpo4 because PolB1 exo- has a 5.1 kcal/mol larger E_a value. PolB1 exo- contains a tighter polymerase active site than Dpo4 and interacts more intensely with a nascent base pair than Dpo4, leading to a higher energy cost in step 3.

For incorrect nucleotide incorporation catalyzed by T7 DNA polymerase (*13*, *14*), *E. coli* DNA polymerase I (*9*), and Dpo4 (*25*), step 4 has been suggested to be the rate-limiting step. Unfortunately, most of these studies (*9*, *13*, *25*) examined the α-thio effect which is largely considered an unreliable criterion (see discussion above) (*40*). On the basis of the α-thio effect of 36 (Figure 4B), step 4 could be rate-limiting for dGTP misincorporation. However, this conclusion is not supported by the large E_a for dATP misincorporation (55 kcal/mol) which indicated step 3, rather than step 4, is rate-limiting. More studies are required to unambiguously identify whether step 3, step 4, or both are rate-limiting during a misincorporation.

Kinetic Implications of PolB1 Interacting with a Processivity Cofactor. According to the rates generated by computer simulation (Figure 3), the processivity of PolB1, a replicative B-family enzyme, was estimated to be 15 at 37 °C which is almost identical to the value (i.e., 16) obtained for Dpo4, a lesion-bypass Y-family enzyme notorious for exhibiting poor processivity (*25*). The processivity of both PolB1 exo- and Dpo4 was reduced by an unexpectedly fast DNA dissociation rate that was subsequently identified to be that of the E·DNA·dNTP intermediate; a similar finding has been observed for HIV-1 RT (*15*, *25*). Furthermore, the two active DNA polymerases of *S. solfataricus* P2 are not inherently processive. To compensate for this functional shortcoming, PolB1 likely associates with a processivity cofactor to increase the enzyme's processivity during genomic replication. Such an effect of accessory proteins on the processivity of several replicative DNA polymerases, including T4 DNA Pol (*54*), T7 DNA Pol (*55*, *56*), and human DNA polymerase γ (*57*), has been reported. For example, when the 140 kDa catalytic subunit of human DNA polymerase γ associates with its 54 kDa accessory subunit, the processivity value increases from 290 to 2250 (*57*). Interestingly, PolB1 has been shown to interact with both the PCNA2 and PCNA3 subunits of the *S. solfataricus* P2 PCNA heterotrimer (*29*). Through its N-terminal domain, PolB1 can be stimulated by PCNA, as processive DNA synthesis is greatly enhanced (*29*). Thus, it will be interesting to determine the kinetic effect of PCNA on DNA polymerization catalyzed by PolB1.

Comparison of Kinetic Parameters of PolB1 and Other DNA Polymerases. Despite the contrasting active sites of PolB1 and Dpo4 (*27*, *58*), the kinetic parameters discerned for these two polymerases are strikingly similar (Table 1) (*25*). The K_d^{DNA} value for PolB1 differs by approximately 6-fold relative to that for Dpo4. Moreover, the most significant difference is the ground-state binding affinity ($1/K_d^{dNTP}$) of an

Table 1: Estimated Kinetic Constants

polymerase	PolB1 exo-	Dpo4	T4 DNA polymerase	T7 DNA polymerase
polymerase family	B	Y	B	A
k_1 (μM^{-1} s^{-1})	24	1.9	85	11
k_{-1} (s^{-1})	0.043	0.02	6	0.2
K_d^{DNA} (nM)	1.8	10.6	70	17.8
k_2 (μM^{-1} s^{-1})	100	100	ND	≥50
k_{-2} (s^{-1})	1100	23000	ND	≥1000
K_d^{dNTP} (μM)	11	230	20	18
k_3 (s^{-1})	8.2	9.4	400	287
k_7 (s^{-1})	0.18	0.41	ND	ND
k_8 (s^{-1})	0.0071	0.004	ND	ND
reaction temperature (°C)	37	37	20	20
reference	this work	(*25*)	(*18*)	(*12*)

incoming nucleotide. For the incorporation of dTTP into D-1 DNA, PolB1 catalyzes this reaction with a 21-fold tighter dNTP binding affinity compared to Dpo4, although their incorporation rates were close (8.2 s^{-1} vs 9.4 s^{-1}). The cellular levels of PolB1 and Dpo4 are similar according to Western blot analysis (*5*); therefore, maintaining low nucleotide concentrations may control the error-prone polymerase activity of Dpo4 on an undamaged DNA template during DNA replication (*24*).

So far, T4 DNA polymerase is the only B-family DNA polymerase with a well-studied kinetic mechanism (*18*−*20*). To serve as another basis for comparison, bacteriophage T7 DNA polymerase is an A-family replicative polymerase with a detailed kinetic mechanism (*12*, *13*). Please note that the kinetic mechanism of T7 DNA Pol was elucidated in the presence of its processivity cofactor, *E. coli* thioredoxin, which is in contrast to the T4 DNA Pol and PolB1 exo- studies. Interestingly, PolB1 exo- binds to DNA with a tighter binding affinity (∼39- and 10-fold) than T4 DNA Pol and T7 DNA Pol under the specified reaction conditions (Table 1) (*12*, *18*). Also noteworthy is the fact that T4 DNA Pol has a dramatically faster k_{-1}; however, this may be in part due to the use of a short primer−template substrate that is not optimal for the enzyme to bind (Table 1) (*18*). Additionally, the fast dissociation rate of T4 DNA Pol may be attenuated by the accessory proteins, gp44, -62, -45, and -32. With regard to dNTP binding, all three replicative polymerases follow the same trend, whereby the K_d^{dNTP} values of correct nucleotides are in the low micromolar range and mismatched nucleotides are in the millimolar range, a difference of almost 3 orders of magnitude (*12*, *13*, *18*, *32*). Thus, regulating the cellular concentrations of nucleotide pools is a natural way to limit mistakes by PolB1 in vivo. The rates of polymerization catalyzed by PolB1 exo- versus the bacteriophages vary widely, but this is largely a function of the temperature profile for each enzyme (Table 1). In the preceding paper (*32*), k_3 for PolB1 exo- was measured to be 92 s^{-1} at a reaction temperature of 50 °C; therefore, it is plausible that catalysis by PolB1 is even faster at the physiological temperature of 80 °C (*32*). In summary, these three replicative polymerases reveal nuances in their kinetic parameters for various elementary steps which stress the importance of defining these numerical values and how related polymerases defy a unified mechanism.

In summary, the forward polymerization pathway of PolB1 exo- has been investigated. Our pre-steady-state kinetic results support a rate-limiting conformational change during nucleotide incorporation. Together with our kinetic studies on Dpo4 (*25*), these kinetic mechanisms provide a foundation for investigating DNA polymerase switching and other complex DNA transactions that occur at the replication fork.

SUPPORTING INFORMATION AVAILABLE

Kinsim and Fitsim analysis (Figure 1) and measurement of the dissociation rate for the E·DNA·dNTP complex at 35 °C (Figure 2). This material is available free of charge via the Internet at http://pubs.acs.org.

REFERENCES

(1) She, Q., Singh, R. K., Confalonieri, F., Zivanovic, Y., Allard, G., Awayez, M. J., Chan-Weiher, C. C., Clausen, I. G., Curtis, B. A., De Moors, A., Erauso, G., Fletcher, C., Gordon, P. M., Heikamp-de Jong, I., Jeffries, A. C., Kozera, C. J., Medina, N., Peng, X., Thi-Ngoc, H. P., Redder, P., Schenk, M. E., Theriault, C., Tolstrup, N., Charlebois, R. L., Doolittle, W. F., Duguet, M., Gaasterland, T., Garrett, R. A., Ragan, M. A., Sensen, C. W., and Van der Oost, J. (2001) The complete genome of the crenarchaeon *Sulfolobus solfataricus* P2. *Proc. Natl. Acad. Sci. U.S.A. 98*, 7835–7840

(2) Boudsocq, F., Iwai, S., Hanaoka, F., and Woodgate, R. (2001) *Sulfolobus solfataricus* P2 DNA polymerase IV (Dpo4): An archaeal DinB-like DNA polymerase with lesion-bypass properties akin to eukaryotic poleta. *Nucleic Acids Res. 29*, 4607–4616

(3) De Felice, M., Medagli, B., Esposito, L., De Falco, M., Pucci, B., Rossi, M., Gruz, P., Nohmi, T., and Pisani, F. M. (2007) Biochemical evidence of a physical interaction between *Sulfolobus solfataricus* B-family and Y-family DNA polymerases. *Extremophiles 11*, 277–282

(4) Lou, H., Duan, Z., Sun, T., and Huang, L. (2004) Cleavage of double-stranded DNA by the intrinsic 3′-5′ exonuclease activity of DNA polymerase B1 from the hyperthermophilic archaeon *Sulfolobus solfataricus* at high temperature. *FEMS Microbiol. Lett. 231*, 111–117

(5) Gruz, P., Shimizu, M., Pisani, F. M., De Felice, M., Kanke, Y., and Nohmi, T. (2003) Processing of DNA lesions by archaeal DNA polymerases from *Sulfolobus solfataricus*. *Nucleic Acids Res. 31*, 4024–4030

(6) Kuchta, R. D., Mizrahi, V., Benkovic, P. A., Johnson, K. A., and Benkovic, S. J. (1987) Kinetic mechanism of DNA polymerase I (Klenow). *Biochemistry 26*, 8410–8417

(7) Kuchta, R. D., Benkovic, P., and Benkovic, S. J. (1988) Kinetic mechanism whereby DNA polymerase I (Klenow) replicates DNA with high fidelity. *Biochemistry 27*, 6716–6725

(8) Dahlberg, M. E., and Benkovic, S. J. (1991) Kinetic mechanism of DNA polymerase I (Klenow fragment): Identification of a second conformational change and evaluation of the internal equilibrium constant. *Biochemistry 30*, 4835–4843.

(9) Eger, B. T., and Benkovic, S. J. (1992) Minimal kinetic mechanism for misincorporation by DNA polymerase I (Klenow fragment). *Biochemistry 31*, 9227–9236.

(10) Frey, M. W., Sowers, L. C., Millar, D. P., and Benkovic, S. J. (1995) The nucleotide analog 2-aminopurine as a spectroscopic probe of nucleotide incorporation by the Klenow fragment of *Escherichia coli* polymerase I and bacteriophage T4 DNA polymerase. *Biochemistry 34*, 9185–9192.

(11) Joyce, C. M., Potapova, O., Delucia, A. M., Huang, X., Basu, V. P., and Grindley, N. D. (2008) Fingers-closing and other rapid conformational changes in DNA polymerase I (Klenow fragment) and their role in nucleotide selectivity. *Biochemistry 47*, 6103–6116.

(12) Patel, S. S., Wong, I., and Johnson, K. A. (1991) Pre-steady-state kinetic analysis of processive DNA replication including complete characterization of an exonuclease-deficient mutant. *Biochemistry 30*, 511–525.

(13) Wong, I., Patel, S. S., and Johnson, K. A. (1991) An induced-fit kinetic mechanism for DNA replication fidelity: Direct measurement by single-turnover kinetics. *Biochemistry 30*, 526–537.

(14) Tsai, Y. C., and Johnson, K. A. (2006) A new paradigm for DNA polymerase specificity. *Biochemistry 45*, 9675–9687.

(15) Kati, W. M., Johnson, K. A., Jerva, L. F., and Anderson, K. S. (1992) Mechanism and fidelity of HIV reverse transcriptase. *J. Biol. Chem. 267*, 25988–25997.

(16) Hsieh, J. C., Zinnen, S., and Modrich, P. (1993) Kinetic mechanism of the DNA-dependent DNA polymerase activity of human immunodeficiency virus reverse transcriptase. *J. Biol. Chem. 268*, 24607–24613.

(17) Zinnen, S., Hsieh, J. C., and Modrich, P. (1994) Misincorporation and mispaired primer extension by human immunodeficiency virus reverse transcriptase. *J. Biol. Chem. 269*, 24195–24202.

(18) Capson, T. L., Peliska, J. A., Kaboord, B. F., Frey, M. W., Lively, C., Dahlberg, M., and Benkovic, S. J. (1992) Kinetic characterization of the polymerase and exonuclease activities of the gene 43 protein of bacteriophage T4. *Biochemistry 31*, 10984–10994

(19) Frey, M. W., Nossal, N. G., Capson, T. L., and Benkovic, S. J. (1993) Construction and characterization of a bacteriophage T4 DNA polymerase deficient in 3′→5′ exonuclease activity. *Proc. Natl. Acad. Sci. U.S.A. 90*, 2579–2583

(20) Wu, P., Nossal, N., and Benkovic, S. J. (1998) Kinetic characterization of a bacteriophage T4 antimutator DNA polymerase. *Biochemistry 37*, 14748–14755

(21) Hariharan, C., and Reha-Krantz, L. J. (2005) Using 2-aminopurine fluorescence to detect bacteriophage T4 DNA polymerase-DNA complexes that are important for primer extension and proofreading reactions. *Biochemistry 44*, 15674–15684

(22) Hariharan, C., Bloom, L. B., Helquist, S. A., Kool, E. T., and Reha-Krantz, L. J. (2006) Dynamics of nucleotide incorporation:

Snapshots revealed by 2-aminopurine fluorescence studies. *Biochemistry 45*, 2836–2844.
(23) Washington, M. T., Prakash, L., and Prakash, S. (2001) Yeast DNA polymerase η utilizes an induced-fit mechanism of nucleotide incorporation. *Cell 107*, 917–927.
(24) Fiala, K. A., and Suo, Z. (2004) Pre-Steady-State Kinetic Studies of the Fidelity of *Sulfolobus solfataricus* P2 DNA Polymerase IV. *Biochemistry 43*, 2106–2115.
(25) Fiala, K. A., and Suo, Z. (2004) Mechanism of DNA Polymerization Catalyzed by *Sulfolobus solfataricus* P2 DNA Polymerase IV. *Biochemistry 43*, 2116–2125.
(26) Fiala, K. A., Sherrer, S. M., Brown, J. A., and Suo, Z. (2008) Mechanistic consequences of temperature on DNA polymerization catalyzed by a Y-family DNA polymerase. *Nucleic Acids Res. 36*, 1990–2001.
(27) Savino, C., Federici, L., Johnson, K. A., Vallone, B., Nastopoulos, V., Rossi, M., Pisani, F. M., and Tsernoglou, D. (2004) Insights into DNA replication: The crystal structure of DNA polymerase B1 from the archaeon *Sulfolobus solfataricus*. *Structure 12*, 2001–2008.
(28) Duggin, I. G., and Bell, S. D. (2006) The chromosome replication machinery of the archaeon *Sulfolobus solfataricus*. *J. Biol. Chem. 281*, 15029–15032.
(29) Dionne, I., Nookala, R. K., Jackson, S. P., Doherty, A. J., and Bell, S. D. (2003) A heterotrimeric PCNA in the hyperthermophilic archaeon *Sulfolobus solfataricus*. *Mol. Cell 11*, 275–282.
(30) Dionne, I., Brown, N. J., Woodgate, R., and Bell, S. D. (2008) On the mechanism of loading the PCNA sliding clamp by RFC. *Mol. Microbiol. 68*, 216–222.
(31) Xing, G., Kirouac, K., Shin, Y. J., Bell, S. D., and Ling, H. (2009) Structural insight into recruitment of translesion DNA polymerase Dpo4 to sliding clamp PCNA. *Mol. Microbiol. 71*, 678–691.
(32) Zhang, L., Brown, J. A., Newmister, S. A., and Suo, Z. (2009) Polymerization Fidelity of a Replicative DNA Polymerase from the Hyperthermophilic Archaeon *Sulfolobus solfataricus* P2. *Biochemistry* (DOI 10.1021/bi900532w).
(33) Eckstein, F. (1985) Nucleoside phosphorothioates. *Annu. Rev. Biochem. 54*, 367–402.
(34) Liu, J., and Tsai, M. D. (2001) DNA polymerase β: Pre-steady-state kinetic analyses of dATPαS stereoselectivity and alteration of the stereoselectivity by various metal ions and by site-directed mutagenesis. *Biochemistry 40*, 9014–9022.
(35) Arnold, J. J., Ghosh, S. K., and Cameron, C. E. (1999) Poliovirus RNA-dependent RNA polymerase (3D(pol)). Divalent cation modulation of primer, template, and nucleotide selection. *J. Biol. Chem. 274*, 37060–37069.
(36) Barshop, B. A., Wrenn, R. F., and Frieden, C. (1983) Analysis of numerical methods for computer simulation of kinetic processes: Development of KINSIM—a flexible, portable system. *Anal. Biochem. 130*, 134–145.
(37) Zimmerle, C. T., and Frieden, C. (1989) Analysis of progress curves by simulations generated by numerical integration. *Biochem. J. 258*, 381–387.
(38) Herschlag, D., Piccirilli, J. A., and Cech, T. R. (1991) Ribozyme-catalyzed and nonenzymatic reactions of phosphate diesters: Rate effects upon substitution of sulfur for a nonbridging phosphoryl oxygen atom. *Biochemistry 30*, 4844–4854.
(39) Fiala, K. A., and Suo, Z. (2004) Mechanism of DNA Polymerization Catalyzed by *Sulfolobus solfataricus* P2 DNA Polymerase IV. *Biochemistry 43*, 2116–2125.
(40) Joyce, C. M., and Benkovic, S. J. (2004) DNA polymerase fidelity: Kinetics, structure, and checkpoints. *Biochemistry 43*, 14317–14324.
(41) Florian, J., Goodman, M. F., and Warshel, A. (2003) Computer simulation of the chemical catalysis of DNA polymerases: Discriminating between alternative nucleotide insertion mechanisms for T7 DNA polymerase. *J. Am. Chem. Soc. 125*, 8163–8177.
(42) Pauling, L. (1946) Molecular Architecture and Biological Reactions. *Chem. Eng. News 24*, 1375–1377.
(43) Radhakrishnan, R., and Schlick, T. (2006) Correct and incorrect nucleotide incorporation pathways in DNA polymerase β. *Biochem. Biophys. Res. Commun. 350*, 521–529.
(44) Washington, M. T., Johnson, R. E., Prakash, L., and Prakash, S. (2003) The mechanism of nucleotide incorporation by human DNA polymerase η differs from that of the yeast enzyme. *Mol. Cell. Biol. 23*, 8316–8322.
(45) Pelletier, H., Sawaya, M. R., Wolfle, W., Wilson, S. H., and Kraut, J. (1996) Crystal structures of human DNA polymerase β complexed with DNA: implications for catalytic mechanism, processivity, and fidelity. *Biochemistry 35*, 12742–12761.
(46) Li, Y., Korolev, S., and Waksman, G. (1998) Crystal structures of open and closed forms of binary and ternary complexes of the large fragment of *Thermus aquaticus* DNA polymerase I: Structural basis for nucleotide incorporation. *EMBO J. 17*, 7514–7525.
(47) Doublie, S., Tabor, S., Long, A. M., Richardson, C. C., and Ellenberger, T. (1998) Crystal structure of a bacteriophage T7 DNA replication complex at 2.2 Å resolution. *Nature 391*, 251–258.
(48) Franklin, M. C., Wang, J., and Steitz, T. A. (2001) Structure of the replicating complex of a pol α family DNA polymerase. *Cell 105*, 657–667.
(49) Johnson, S. J., Taylor, J. S., and Beese, L. S. (2003) Processive DNA synthesis observed in a polymerase crystal suggests a mechanism for the prevention of frameshift mutations. *Proc. Natl. Acad. Sci. U.S.A. 100*, 3895–3900.
(50) Garcia-Diaz, M., Bebenek, K., Krahn, J. M., Kunkel, T. A., and Pedersen, L. C. (2005) A closed conformation for the Pol λ catalytic cycle. *Nat. Struct. Mol. Biol. 12*, 97–98.
(51) Wong, J. H., Fiala, K. A., Suo, Z., and Ling, H. (2008) Snapshots of a Y-family DNA polymerase in replication: Substrate-induced conformational transitions and implications for fidelity of Dpo4. *J. Mol. Biol. 379*, 317–330.
(52) Rothwell, P. J., Mitaksov, V., and Waksman, G. (2005) Motions of the fingers subdomain of klentaq1 are fast and not rate limiting: Implications for the molecular basis of fidelity in DNA polymerases. *Mol. Cell 19*, 345–355.
(53) Pal, S. K., and Zewail, A. H. (2004) Dynamics of water in biological recognition. *Chem. Rev. 104*, 2099–2123.
(54) Mace, D. C., and Alberts, B. M. (1984) Characterization of the stimulatory effect of T4 gene 45 protein and the gene 44/62 protein complex on DNA synthesis by T4 DNA polymerase. *J. Mol. Biol. 177*, 313–327.
(55) Tabor, S., Huber, H. E., and Richardson, C. C. (1987) *Escherichia coli* thioredoxin confers processivity on the DNA polymerase activity of the gene 5 protein of bacteriophage T7. *J. Biol. Chem. 262*, 16212–16223.
(56) Huber, H. E., Tabor, S., and Richardson, C. C. (1987) *Escherichia coli* thioredoxin stabilizes complexes of bacteriophage T7 DNA polymerase and primed templates. *J. Biol. Chem. 262*, 16224–16232.
(57) Johnson, A. A., Tsai, Y., Graves, S. W., and Johnson, K. A. (2000) Human mitochondrial DNA polymerase holoenzyme: Reconstitution and characterization. *Biochemistry 39*, 1702–1708.
(58) Ling, H., Boudsocq, F., Woodgate, R., and Yang, W. (2001) Crystal structure of a Y-family DNA polymerase in action: A mechanism for error-prone and lesion-bypass replication. *Cell 107*, 91–102.